The Expanding Role of Deep Learning Reconstruction in Prostate MRI

Paulo Gil Agostinho[1], Ana Raquel Clemente[1], Filipe Caseiro Alves[1], Marcel Dominik Nickel[3], Livia Sacchetto de Andrade[2], Marisa Gonçalves[2], Cristiana Araújo[2], André Barbosa[2]

[1]Hospital da Luz, Coimbra, Portugal
[2]Siemens Healthineers, Portugal
[3]Siemens Healthineers, Erlangen, Germany

Introduction

Prostate cancer is one of the most prevalent oncological pathologies, with the highest incidence observed in Europe [1]. If death rates remain unchanged, the International Agency for Research on Cancer predicts that the burden will rise to 1.7 million new cases and 499,000 deaths by 2030 [1]. The primary diagnosis of this disease is based on prostate-specific-antigen (PSA) screening, and biopsy. Due to the low specificity of PSA screening (36%), false positives are commonly present in the results, as an elevated PSA does not necessarily indicate the presence of cancer [2, 3]. Furthermore, a normal value can neither exclude the presence nor the potential development of a tumor [2, 3].

Because prostate cancer is multifocal in almost 85% of cases [4], ultrasound-guided biopsy may underestimate the extent and grade of the tumor, which may result in an update of the Gleason score after prostatectomy [4]. Additionally, since prostate biopsy is not directed at any specific lesion, it can lead to reduced diagnostic accuracy, particularly in anterior prostate lesions and in lesions located in the apex. Finally, ultrasound biopsy has a negative predictive value (NPV) of 70 to 80%, which means that 20 to 30% of patients with a negative biopsy result may still have prostate cancer [5]. It has been observed that men with continuously high levels of PSA can have negative systematic results in biopsy [6, 7].

This means magnetic resonance imaging (MRI) plays a decisive role in prostate cancer diagnosis. It offers reliable visualization, which is potentially significant for prostate cancer diagnosis, and provides information for staging tumor extent, monitoring treatment response, and guiding focal therapies. MRI has also shown advantages in terms of improving the selection of patients who need to undergo biopsy, and facilitating the targeting of lesions during biopsy.

MRI is therefore an indispensable tool for detecting prostate cancer, especially in men with continuously high levels of PSA despite a negative systematic biopsy [6, 7]. With the huge growth in the volume of exams and the recent recommendations by the Council of the European Union to facilitate a more targeted and less invasive screening by using MRI as a follow-up for PSA screening, there is an urgent need to find a way to provide faster MRI examinations. Also, according to the guidelines on prostate cancer from the European Association of Urology, MRI scanning is strongly recommended before biopsy [8].

The increasing application of deep learning (DL) algorithms, such as convolutional neural networks (CNNs), offers fascinating prospects for the future of both MRI and medicine in general [9]. The use of DL techniques in MRI can help overcome several challenges by reducing acquisition times, increasing spatial and contrast resolution, and thereby improving the overall study quality [10].

The main objective of this study is to determine the role of DL reconstruction algorithms in prostate MRI examinations and their impact on clinical practice and prostate cancer diagnosis.

MRI technique

With conventional reconstruction methods, an acquisition can only be accelerated by accepting compromises between image resolution and signal-to-noise ratio (SNR). In general, acquisition speed, image resolution, and SNR are tightly linked and increasing one of the three automatically has a negative effect on at least one of the other two. The use of receive arrays and parallel imaging has been an important breakthrough in MR image reconstruction and is an essential part of clinical routine in MRI.

Parallel imaging, however, usually comes at the price of higher image noise, especially in regions far from the receiving coil elements. This results in inhomogeneous noise distribution, especially if high acceleration factors are used. In recent years, artificial intelligence (AI) technologies have made their appearance in various research applications and products. In particular, the use of deep neural networks has proven to be helpful when trying to address the limitations of conventional MR image reconstruction, even in routine 2D imaging. DL image reconstruction has the potential to tackle all three limiting factors of MR imaging simultaneously: image resolution, SNR, and acquisition speed [11].

With the introduction of DL reconstruction, convolutional networks were inserted into the image formation process, which now also involves image enhancement steps interleaved with conventional parallel imaging [12].

In DL reconstruction, the image reconstruction comprises a fixed iterative scheme or variational network, alternating between data consistency and a CNN-based regularization. The regularization model architecture is based on a novel hierarchical design of an iterative network that repeatedly decreases and increases the resolution of the feature maps, allowing for a more memory-efficient model than conventional CNNs.

Coil sensitivity maps are estimated from the calibration data in advance as a pre-processing step. For image reconstruction, undersampled *k*-space data, bias field correction maps, and coil sensitivity maps are inserted into the variational network [13].

Materials and methods

A total of 67 patients with an average PSA of 6.3 ng/mL ([0.6;12.71] ng/mL) underwent a multiparametric prostate MRI examination in a clinical 3T scanner (MAGNETOM Vida, Siemens Healthcare, Erlangen, Germany) in supine position with an 18-channel body array and a 32-channel spine array. In addition to diffusion-weighted and dynamic contrast-enhanced sequences, we used two different T2-weighted sequences: One was the standard T2 turbo spin-echo (TSE) sequence and the other was a prototype of a DL-accelerated T2 TSE sequence, which the vendor, Siemens Healthineers, has since productized as Deep Resolve Boost TSE. Both sequences were used to acquire images in the three conventional orientations (transversal, sagittal and coronal). The average total time of acquisition was 10 minutes for the T2 standard sequence and 4:50 minutes for the DL T2 sequence (for detailed parameters, see Table 1).

Sequence	**T2 TSE**					
Orientation	**Sagittal**		**Axial**		**Coronal**	
Type	Standard	DL	Standard	DL	Standard	DL
Acquisition time (TA) (min:sec)	02:30	01:28	05:05	01:49	02:32	01:30
Field of view (FOV) (mm x mm)	150 x 100	160 x 100	180 x 100	180 x 100	160 x 100	160 x 100
Matrix size (mm)	224 x 320	222 x 320	269 x 384	269 x 384	224 x 320	224 x 320
Repetition time (TR) (msec)	6000	6290	8940	5950	6000	8060
Echo time (TE) (msec)	123	101	116	104	123	101
Slice thickness (mm)	3	3	3	3	3	3
Acceleration factor	2	2	2	3	3	2
Number of averages	2	1	3	1	2	1
Number of slices	28	29	38	35	27	28

Table 1: Acquisition parameters for the standard and DL T2 sequences.

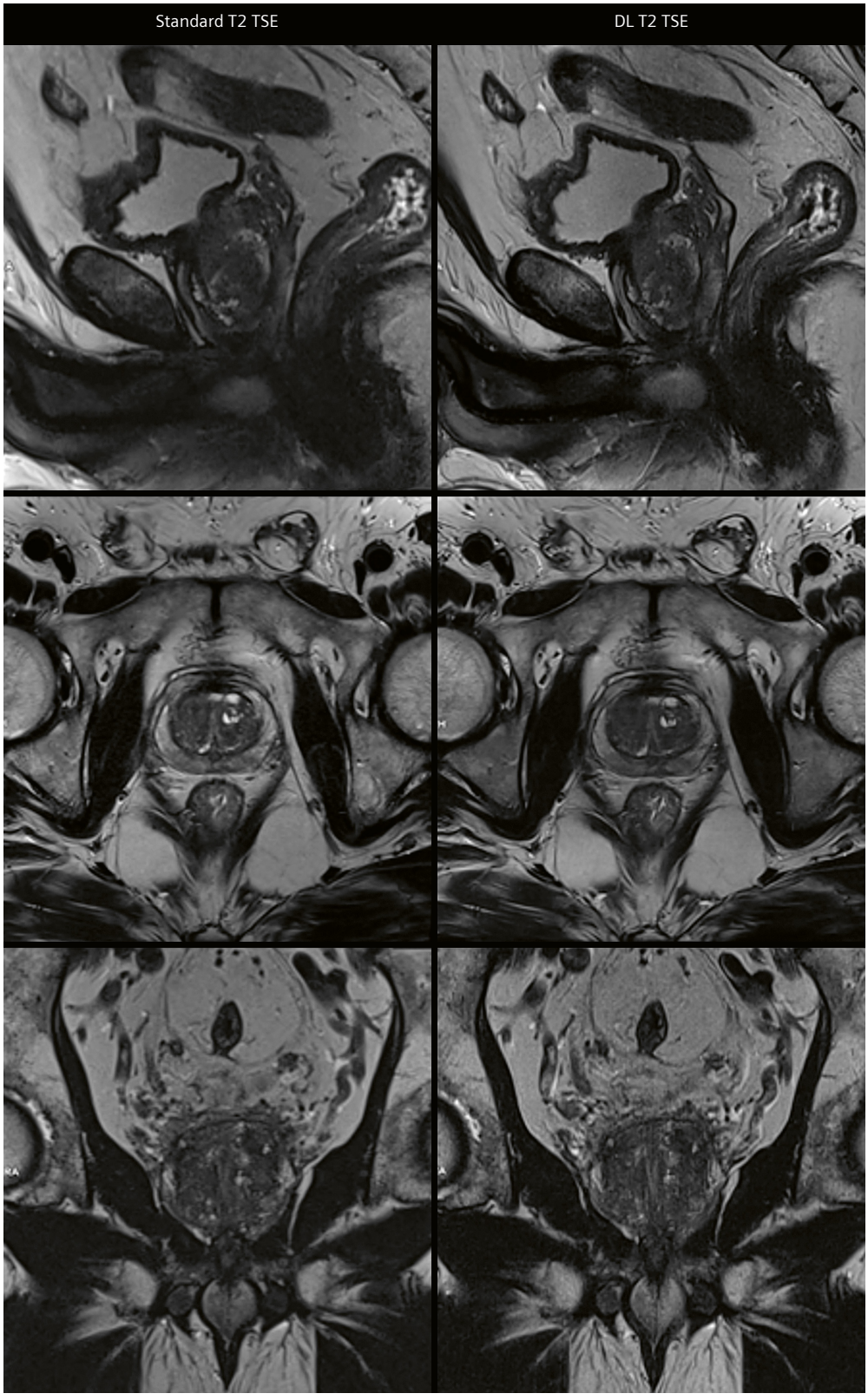

1 Comparison between the standard T2 TSE (left) and DL T2 TSE (right) sequences. The DL sequence reduces the acquisition time by 52% and improves image quality.

Quantitative image analysis

We compared the two sequences in 67 patients in terms of acquisition time (Fig. 1), signal-to-noise ratio (SNR) (Fig. 2A), and contrast-to-noise ratio (CNR) (Fig. 2B) using the formulas

$$SNR = \frac{S_1}{s}$$

$$CNR = \frac{S_1 - S_2}{s}$$

where S_1 and S_2 are the average signal intensity measured in the regions of interest (ROIs), which were placed in the prostate peripheral zone and in the obturator internus muscle, respectively; and s is the standard deviation of the signal intensity of S_2. The signal intensity of S_2 is the background noise, since the signal intensity of the obturator internus muscle is homogeneous and low.

Qualitative image analysis

The image quality of the standard and DL T2 sequences was evaluated by a local radiologist, who compared the images in four anatomical regions of the prostate (peripheral zone, internal sphincter, mesorectal fascia, prostatic capsule, and peripheral prostatic lesion) and the presence of lesion. The image quality was rated using a 5-point Likert scale.

Results

The DL TSE T2 sequence was successfully used in all 67 cases and was compared with the standard T2 TSE sequence in terms of acquisition time, SNR, and CNR. The acquisition time difference between the two sequences (with and without the DL algorithm) was evident, with the DL sequence showing a significant reduction in 97% of the cases. In 40 cases, we observed a 70% reduction; in 25 cases, the time reduction was greater than 65%; in the remaining two cases, we observed a roughly 50% reduction in acquisition time. It is also worth mentioning that the time needed to plan the sequence was also reduced when using the DL sequence, since there was no need to adjust the number of slices in 63% of the cases. By contrast, the number of slices needed to be adjusted in 66% of the cases when using the standard sequence. This is because the DL sequence allows a larger predefined number of slices while maintaining a short scan time, which proved to be adequate for patients with enlarged prostates. In the DL-sequence images, both the SNR and CNR were

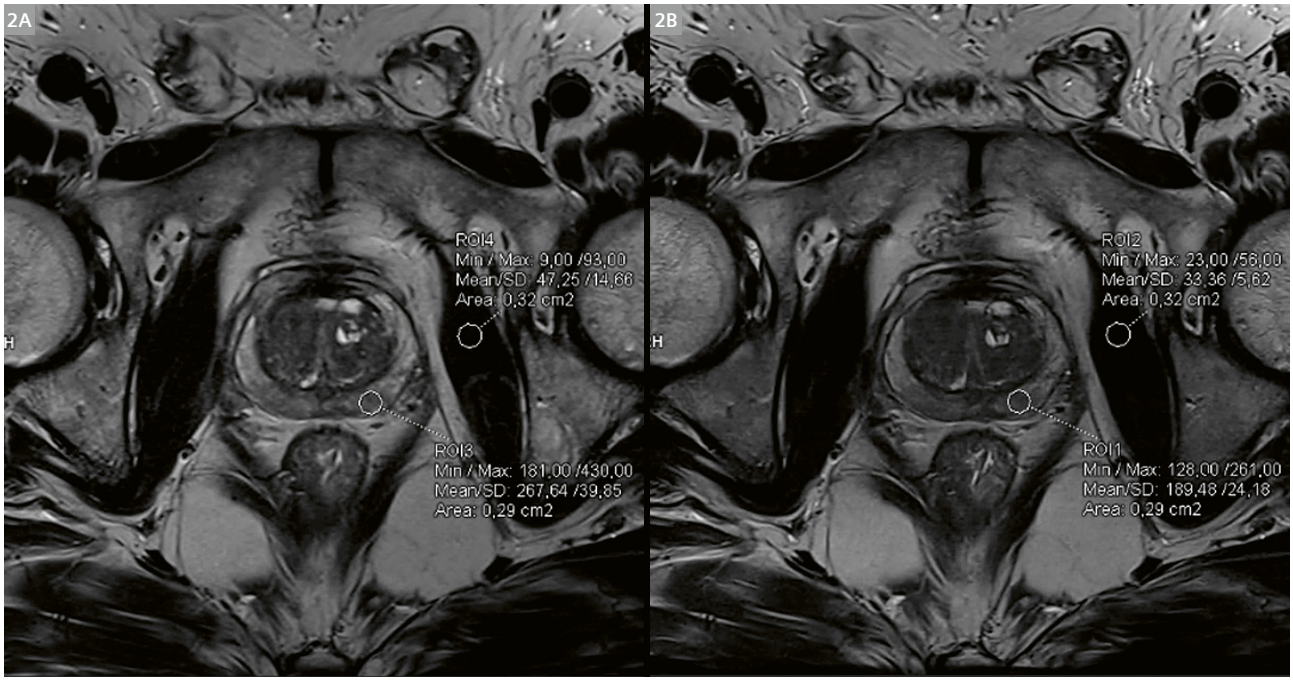

2 Evaluation of SNR and CNR using the average signal intensity of ROIs placed in the peripheral prostate and in the obturator internus muscle. **(2A)** Standard T2: SNR = 19.1, CNR = 15.7; **(2B)** DL T2: SNR =33.7, CNR = 27.77

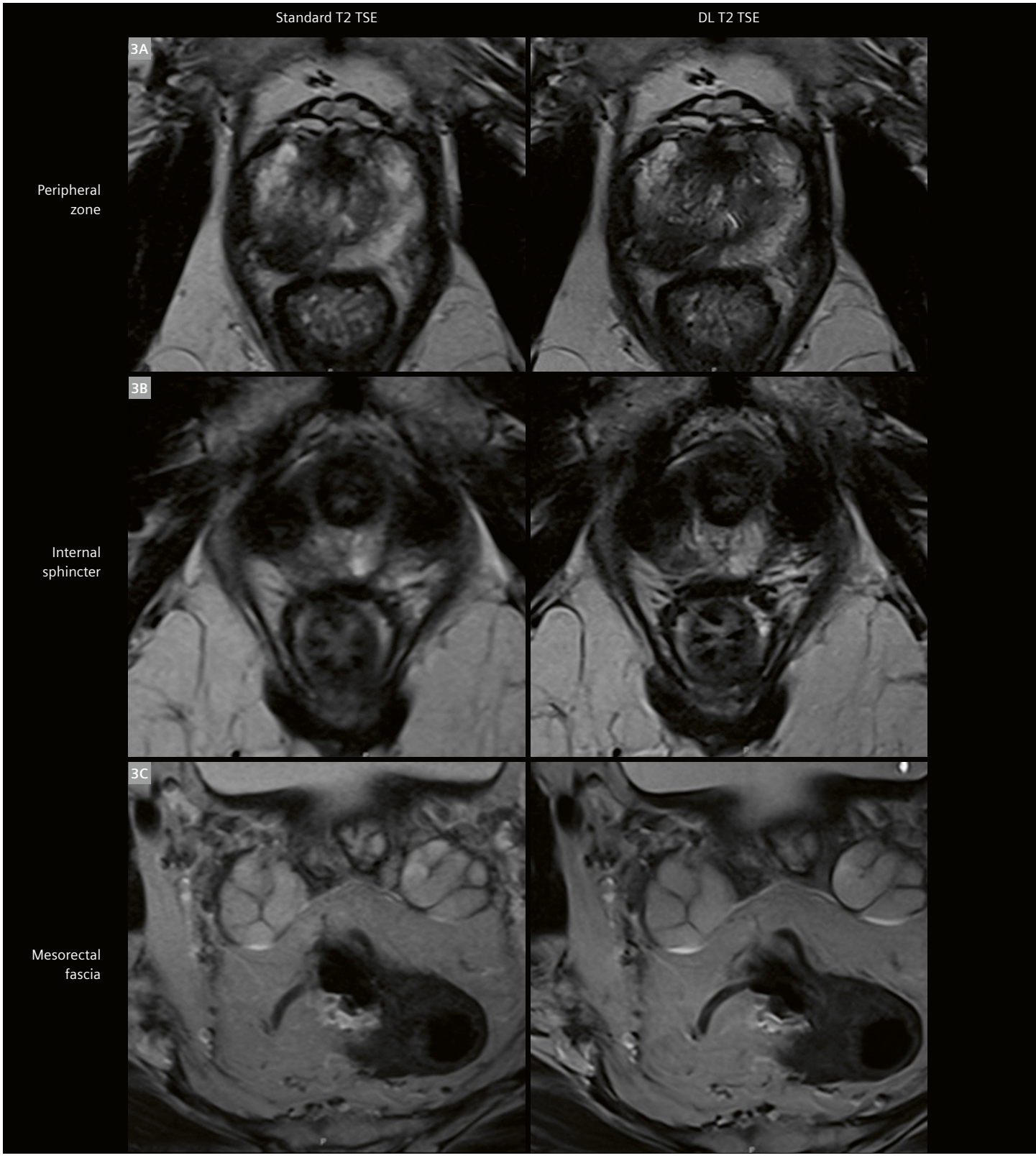

3 Standard T2 TSE versus DL T2 TSE in the peripheral zone **(3A)**, internal sphincter **(3B)**, mesorectal fascia **(3C)**, prostatic capsule **(3D)**, and focal lesion conspicuity **(3E)**, PI-RADS score **(3F)**.

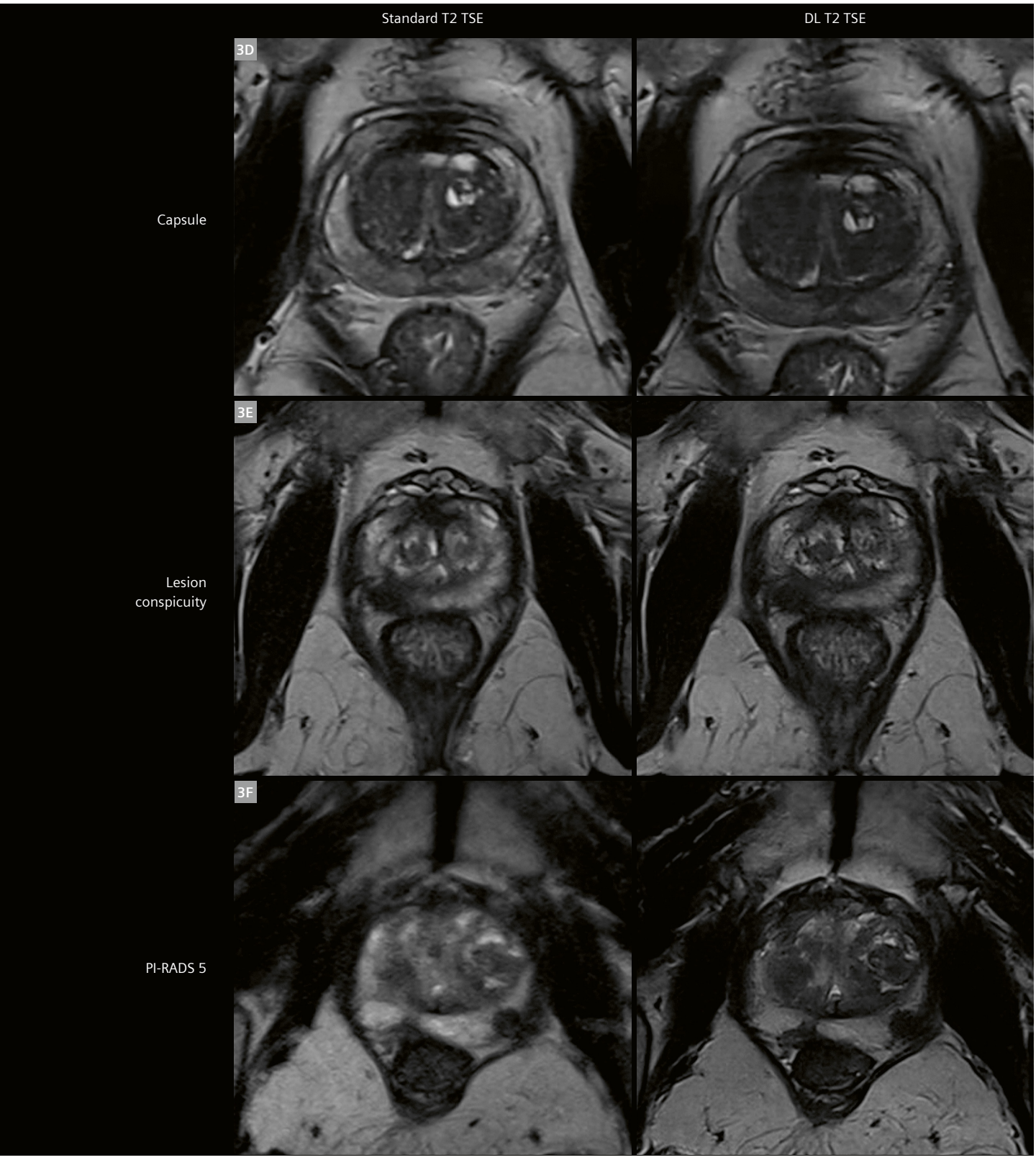
Standard T2 TSE
DL T2 TSE
3D
Capsule
3E
Lesion conspicuity
3F
PI-RADS 5

higher in most of the cases, with SNR being higher in 90% of them and CNR in 88%. In very few cases, the DL images presented lower SNR and CNR than the standard images. This can be explained by previously diagnosed prostatitis, a clinical condition known to correlate with low signal in the prostatic peripheral zone.

The quantitative and qualitative results of the comparison between the standard and the DL sequences are summarized in Table 2. The positive difference in median values of SNR and CNR shows a quantitative increase in image quality of the DL sequence, which can be achieved with significantly shorter TA, as shown by the negative median TA difference. Moreover, repeated measurements of SNR, CNR, and TA are moderately and positively correlated (respectively, rS = 0.527, rS = 0.510, and rS = 0.418). In addition, there was a median increase of one Likert point in favor of the DL sequence, related to the identification of each of the five characteristics evaluated for attaining lesion conspicuity, ($p < 0.001$ for each of the five comparisons).

The image quality of the DL sequence was consistently evaluated as being equal to or better than the standard sequence in all anatomical areas. In the peripheral zone, it was considered to have better image quality in 85% of the cases; in the internal sphincter, this was 61%; in the mesorectum, 43%; and in the prostatic capsule, 79%. In the remaining cases, the image quality of the DL sequence was considered to be the same as that provided by the standard sequence.

	Median difference (DL-Std)	p-value
SNR	9.71	< 0.001
CNR	7.14	< 0.001
TA (seconds)	-211	< 0.001
Peripheral prostate	1	< 0.001
Internal sphincter	1	< 0.001
Mesorectal fascia	1	< 0.001
Prostatic capsule	1	< 0.001
Peripheral prostate lesion	1	< 0.001

Table 2: Comparison of results from the standard (Std T2) and deep learning (DL T2) sequences. There is an increase in SNR of 9.71 (IQR (interquartile range): [3.71; 19.01]; $p < 0.001$) and in CNR of 7.14 (IQR: [1.80; 16.89]; $p < 0.001$), a median decrease of 211s (IQR: [186; 236]; $p < 0.001$) in the time of acquisition, corresponding to a reduction of 70.3%, when using the DL sequence. Median difference refers to the image quality evaluation (Likert scale) in the regions evaluated between the DL and standard sequences. All regions present are rated one point higher when using the DL sequence. Statistical analysis: Wilcoxon matched-pairs test. Association between standard T2 and DL T2 was analyzed using Spearman's rank-order correlation. Statistical tests were evaluated at a 5% significance level. Analysis was performed in SPSS Statistics, version 27 (IBM, Armonk, New York, USA).

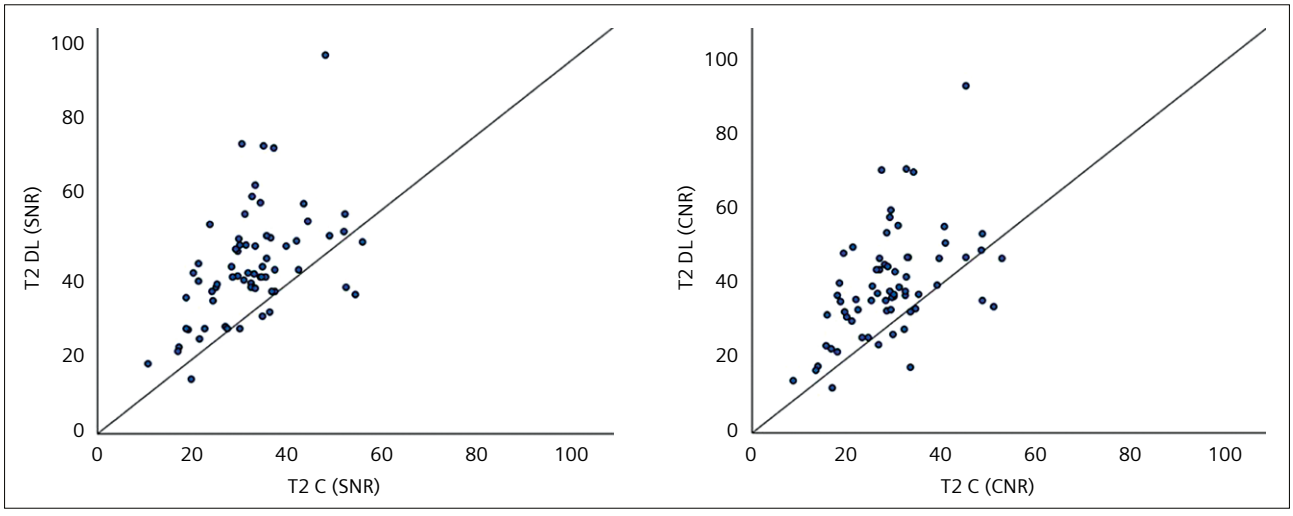

4 Distribution of SNR and CNR of the DL sequence (T2 DL) against the standard sequence (T2 C). The DL sequence yielded higher SNR and CNR values for most measurements.

Additionally, since 47 cases had lesions in the peripheral zone, the signal intensity in the lesions was compared for the two sequences. Here, the DL sequence showed higher signal intensity in the lesion in 53% of the cases, equal signal intensity in 42%, and lower signal intensity in 4%.

Discussion

Deep learning reconstruction is a very active field of research and is currently being translated into clinical practice. It shows great potential for the future of MR imaging, including denoising and artifact reduction [10]. Most importantly, faster and better MRI will make prostate cancer screening more efficient by enabling a more accurate diagnosis and reaching a broader population.

Deep learning reconstruction of T2 TSE in the prostate enabled an extraordinary reduction in acquisition time, while improving or maintaining SNR and CNR. The overall image quality was also improved in different anatomical regions such as the peripheral zone, internal sphincter, mesorectal fascia, and prostatic capsule. This was in addition to an improvement in the identification of peripheral zone lesions.

References

1 International Agency for Research on Cancer. European Urology – International Variation in Prostate Cancer Incidence and Mortality Rates [Internet]. Lyon, France: International Agency for Research on Cancer; 2012 [Accessed on May 3, 2023]. Available from: ↗ https://www.iarc.who.int/news-events/european-urology-international-variation-in-prostate-cancer-incidence-and-mortality-rates/

2 Barentsz JO, Richenberg J, Clements R, Choyke P, Verma S, Villeirs G, et al. ESUR Prostate MR guidelines 2012. Eur Radiol. 2012;22(4):746–757.

3 Hambrock T, Somford DM, Hoeks C, Bouwense SA, Huisman H, Yakar D, et al. Magnetic resonance imaging guided prostate biopsy in men with repeat negative biopsies and increased prostate specific antigen. J Urol. 2010;183(2):520–527.

4 Bonekamp D, Jacobs MA, El-Khouli R, Stoianovici D, Macura KJ. Advancements in MR imaging of the prostate: from diagnosis to interventions. Radiographics 2011;31(3):677–703.

5 Ahmed HU, Kirkham A, Arya M, Illing R, Freeman A, Allen C, et al. Is it time to consider a role for MRI before prostate biopsy? Nat Rev Clin Oncol. 2009;6(4):197–206.

6 Sonn GA, Chang E, Natarajan S, Margolis DJ, Macairan M, Lieu P, et al. Value of targeted prostate biopsy using magnetic resonance-ultrasound fusion in men with prior negative biopsy and elevated prostate-specific antigen. Eur Urol. 2014;65(4):809–815.

7 Hoeks CM, Schouten MG, Bomers JG, Hoogendoorn SP, Hulsbergen-van de Kaa CA, Hambrock T, et al. Three-Tesla magnetic resonance-guided prostate biopsy in men with increased prostate-specific antigen and repeated, negative, random, systematic, transrectal ultrasound biopsies: detection of clinically significant prostate cancers. Eur Urol. 2012;62(5):902–909.

8 European Association of Urology. Prostate Cancer [Internet]. Arnhem, the Netherlands: European Association of Urology; 2023 [Accessed on May 3, 2023]. Available from: https://uroweb.org/guidelines/prostate-cancer

9 Kim J, Hong J, Park H. Prospects of deep learning for medical imaging. Precis Futur Med. 2018;2(2):37–52.

10 Suzuki K. Overview of deep learning in medical imaging. Radiol Phys Technol. 2017;10(3):257–273.

11 Behl N. Deep Resolve – Mobilizing the Power of Networks. MAGNETOM Flash. 2021;78(1):29–35. ↗ https://marketing.webassets.siemens-healthineers.com/2efe552ddbfa9372/3bcd31c7597b/Behl_DeepResolve_MAGNETOM_Flash_78_ISMRM_2021.pdf

12 Mulé S, Massire A, Zerbib P, Nickel D, Luciani A. Fast and Reliable Liver Imaging Using Deep Learning HASTE. MAGNETOM Flash. 2021;79(2):28–31. ↗ https://marketing.webassets.siemens-healthineers.com/64a9a07fa3ff23f6/2a243add4eb7/MAGNETOM_Flash_79_RSNA_2021.pdf

13 Herrmann J, Lingg A, Kündel M, Gassenmaier S, Afat S, Al-Mansour H, et al. Clinical Implementation of Deep Learning Accelerated HASTE and TSE. MAGNETOM Flash. 2021;70(2):23–27. ↗ https://marketing.webassets.siemens-healthineers.com/be50dfa900db3e9f/b495fd2d0a32/Othman_Herrmann_DL-HASTE_TSE_RSNA-2021.pdf

Contact

Filipe Caseiro Alves, M.D., Ph.D.
Hospital da Luz Coimbra
Praceta Robalo Cordeiro, 1
3020-479 Coimbra
Portugal
luis.caseiro.alves@hospitaldaluz.pt

Paulo Gil Agostinho, M.D.
Hospital da Luz Coimbra
Praceta Robalo Cordeiro, 1
3020-479 Coimbra
Portugal
paulo.gil.agostinho@hospitaldaluz.pt